

References and Notes

1. F. R. N. Nabarro, *Theory of Crystal Dislocations* (Clarendon Press, Oxford, 1967).
2. D. Hughes, D. C. Chrzan, Q. Liu, N. Hansen, *Acta Mater.* **45**, 105 (1997).
3. P. Rudolph, *Cryst. Res. Technol.* **40**, 7 (2005).
4. D. Hughes, N. Hansen, *Phys. Rev. Lett.* **87**, 135503 (2001).
5. U. Essmann, *Phys. Status Solidi* **12**, 707 (1965).
6. J. W. Steeds, *Proc. R. Soc. London Ser. A* **292**, 343 (1966).
7. B. Bay, N. Hansen, D. Hughes, D. Kuhlmann-Wilsdorf, *Acta Metall. Mater.* **40**, 205 (1992).
8. P. Cizek, *Scripta Mater.* **45**, 815 (2001).
9. M. Wilkens, *Phys. Status Solidi A* **2**, 359 (1970).
10. M. A. Krivogla, *Theory of X-ray and Neutron Scattering by Real Crystals* (Plenum, New York, 1969).
11. H. Mughrabi, T. Ungar, W. Kienle, M. Wilkens, *Philos. Mag. A* **53**, 793 (1986).
12. R. I. Barabash, P. Klimanek, *J. Appl. Cryst.* **32**, 1050 (1999).
13. H. F. Poulsen, *Three-Dimensional X-ray Diffraction Microscopy* (Springer, Berlin, 2004).
14. E. M. Lauridsen, S. Schmidt, R. M. Suter, H. F. Poulsen, *J. Appl. Cryst.* **34**, 744 (2001).
15. L. Margulies, G. Winther, H. F. Poulsen, *Science* **291**, 2392 (2001).
16. B. C. Larson, W. Yang, G. E. Ice, J. D. Budai, T. Z. Tischler, *Nature* **415**, 887 (2002).
17. E. Göttler, *Philos. Mag.* **28**, 1057 (1973).
18. A. S. Argon, P. Haasen, *Acta Metall. Mater.* **41**, 3289 (1993).
19. M. E. Kassner, M. T. Perez-Prado, M. Long, K. S. Vecchio, *Metall. Mater. Trans. A* **33**, 311 (2002).
20. F. B. Prinz, A. S. Argon, *Acta Metall.* **32**, 1021 (1984).
21. W. D. Nix, J. C. Gibeling, D. A. Hughes, *Metall. Trans. A* **16A**, 2215 (1985).
22. M. Zehetbauer, *Acta Metall. Mater.* **41**, 589 (1993).
23. Y. Estrin, L. Tóth, Y. Brechet, A. Molinari, *Acta Mater.* **46**, 5509 (1998).
24. F. Roters, D. Raabe, G. Gottstein, *Acta Mater.* **48**, 4181 (2000).
25. P. Hähner, *Acta Mater.* **44**, 2345 (1996).
26. Q. Liu, N. Hansen, *Proc. R. Soc. Lond. A* **454**, 2555 (1998).
27. U. Essmann, *Phys. Status Solidi* **3**, 932 (1963).
28. H. Mughrabi, *Philos. Mag.* **23**, 869 (1971).
29. The sample preparation was performed by G. Christiansen, and the EM studies were performed by Q. Xing. This work was supported by the Danish National Research Foundation and the Danish Natural Science Research Council. Use of the Advanced Photon Source was supported by the U.S. Department of Energy, Basic Energy Sciences, Office of Science, under contract no. W-31-109-Eng-38.

Supporting Online Material

www.sciencemag.org/cgi/content/full/312/5775/889/DC1

Materials and Methods

Fig. S1

Movies S1 and S2

21 December 2005; accepted 16 March 2006

10.1126/science.1124141

Simultaneous Negative Phase and Group Velocity of Light in a Metamaterial

Gunnar Dolling,^{1*} Christian Enkrich,¹ Martin Wegener,^{1,2} Costas M. Soukoulis,^{3,4} Stefan Linden²

We investigated the propagation of femtosecond laser pulses through a metamaterial that has a negative index of refraction for wavelengths around 1.5 micrometers. From the interference fringes of a Michelson interferometer with and without the sample, we directly inferred the phase time delay. From the pulse-envelope shift, we determined the group time delay. In a spectral region, phase and group velocity are negative simultaneously. This means that both the carrier wave and the pulse envelope peak of the output pulse appear at the rear side of the sample before their input pulse counterparts have entered the front side of the sample.

The propagation of waves through dispersive media often leads to surprising or counterintuitive behavior (1). For the case of positive-refractive-index media in electrodynamics, where the phase velocity v_{phase} is positive (in the forward direction), the group velocity v_{group} can become negative in the regime of anomalous dispersion. As a result, the peak of a temporally long Gaussian pulse can appear at the rear side of a sample before the peak of the Gaussian input pulse has entered the front side of the sample (2). This phenomenon has been directly observed (3) on an excitonic absorption resonance in a GaP:N semiconductor sample by time resolving the transmission of a picosecond optical pulse. Further experiments along these lines, e.g., on

positive-index systems with gain (4–6), have confirmed this behavior. It has been thoroughly discussed (2) that superluminal or even negative group velocities are not at all in conflict with relativity or causality, essentially because the peak of the output pulse is not a cause of the peak of the input pulse. In other words, even though input and output pulses can have the same Gaussian shape, reshaping of the pulse envelope is of crucial importance.

Here we report results of corresponding experiments on negative-refractive-index materials. These highly unusual materials have only recently become available (7–9), with the optical regime becoming accessible only within the past year (10–14). The phase velocity in these materials is negative. We directly measured both group and phase velocity by propagating a femtosecond laser pulse through a negative-index metamaterial and then time resolving the transmitted pulse using interferometry. These experiments are the negative-index counterpart of the above experiments for positive-index materials (3–6), where $v_{\text{phase}} > 0$ and $v_{\text{group}} < 0$. We found conditions where $v_{\text{phase}} < 0$ and $v_{\text{group}} < 0$, and others where $v_{\text{phase}} < 0$ and $v_{\text{group}} > 0$. Together with the usual situation of $v_{\text{phase}} > 0$

and $v_{\text{group}} > 0$, all four sign combinations have now been observed in direct experiments. For all four sign combinations, the

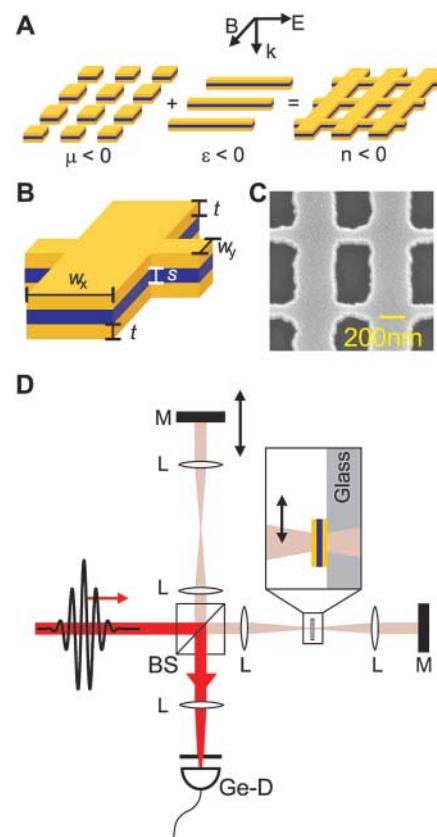


Fig. 1. (A) Scheme of the negative-index metamaterial design and polarization configuration used here. **E** is the incident electric-field vector, **B** the incident magnetic-field vector, and **k** the incident wave vector of light. (B) Definition of parameters: $t = 25$ nm, $s = 35$ nm, $w_x = 307$ nm, $w_y = 100$ nm, and a square lattice with lattice constant $a = 600$ nm. The metamaterial thickness is $d = 2t + s = 85$ nm. (C) Top-view electron micrograph of the corresponding structure. (D) Scheme of the experimental setup. M, mirror; L, lens; BS, beam splitter; Ge-D, germanium photodetector.

¹Institut für Angewandte Physik und Deutsche Forschungsgemeinschaft—Center for Functional Nanostructures, Universität Karlsruhe (TH), Wolfgang-Gaede-Straße 1, D-76131 Karlsruhe, Germany. ²Institut für Nanotechnologie, Forschungszentrum Karlsruhe in der Helmholtz-Gemeinschaft, D-76021 Karlsruhe, Germany. ³Ames Laboratory and Department of Physics and Astronomy, Iowa State University, Ames, IA 50011, USA. ⁴Institute of Electronic Structure and Laser—Foundation for Research and Technology Hellas, and Department of Materials Science and Technology, University of Crete, 71110 Heraklion, Crete, Greece.

*To whom correspondence should be addressed. E-mail: gunnar.dolling@physik.uni-karlsruhe.de

Poynting vector is positive, i.e., along the forward direction.

The negative-index metamaterial samples used in our experiments closely follow a design proposed theoretically in (10) and first realized experimentally in (11). For the polarization configuration sketched in Fig. 1, the material can be thought of as consisting of double-plate (or double-wire) pairs (13, 14), which provide the negative magnetic permeability μ , and long metal wires, which act as a diluted Drude metal. Below the plasma frequency, the latter correspond to an electric permittivity $\epsilon < 0$. The combination of $\mu < 0$ and $\epsilon < 0$ leads to a negative real part of the refractive index n (15). Our samples were fabricated using standard electron-beam lithography and electron-beam evaporation of the constituent materials. In total, we fabricated 60 different negative-index samples on glass substrate covered with a 5-nm thin film of indium-tin-oxide (ITO). Each sample has a footprint of $100\text{ }\mu\text{m} \times 100\text{ }\mu\text{m}$. The sample parameters of the sample discussed below are given in Fig. 1, A to C. An overview of the measured and calculated (16) optical transmittance and reflectance spectra is given in Fig. 2. Here, the gold dielectric function is described by the Drude model with plasma frequency $\omega_p = 1.32 \times 10^{16}\text{ s}^{-1}$ and collision frequency $\omega_c = 1.2 \times 10^{14}\text{ s}^{-1}$. These values are obtained from a fit of the Drude model to the measured complex permittivity of thin gold films (17) in the near-infrared. The refractive index of the glass substrate is $n = 1.5$, and that of the MgF_2 spacer layer is $n = 1.38$. Experiment and theory in Fig. 2 are found to agree very well.

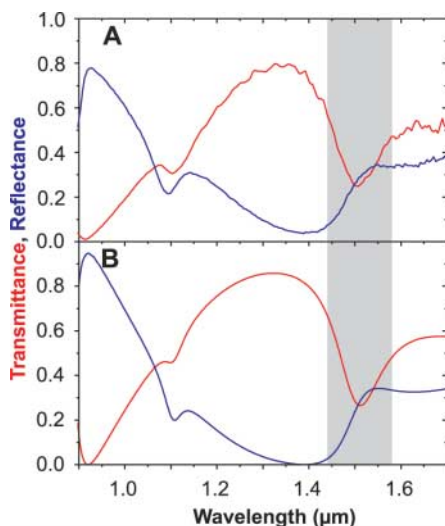


Fig. 2. Transmittance (red) and reflectance (blue) spectra for the polarization configuration and sample shown in Fig. 1. (A) Measurements with a white-light source. (B) Theory. To guide the eye, the total spectral region shown in Fig. 4 is highlighted by the gray area.

From the calculated spectra, we have retrieved (18) the effective metamaterial parameters and we found a negative real part of the refractive index, $\text{Re}(n) < 0$ (see below). As expected from theory (10), we do not obtain $\text{Re}(n) < 0$ for the orthogonal linear polarization.

To perform phase-sensitive experiments on these samples, different interferometer types can be used; for example, a Michelson interferometer or a Mach-Zehnder interferometer. Our setup (Fig. 1D) is essentially a compact Michelson interferometer (not actively stabilized), into one arm of which we can insert the sample. 170-fs, transform-limited Gaussian pulses from an optical parametric oscillator (OPO) that are tunable around 1500-nm wavelength are sent into this interferometer. The output of the interferometer is recorded as a function of the length of one of the interferometer arms, which can immediately be translated into an interferometer time delay. When inserting the sample, the interferogram shifts on the time-delay axis. The shift of its envelope is determined by the sample group velocity. The shift of the rapidly oscillating fringes contains information on the sample phase velocity, provided that two conditions are satisfied: (i) To infer unambiguously the phase velocity from a

phase delay, one must ensure that the phase delay is smaller than one period of light. This condition translates into “thin” samples. For our conditions, the anticipated maximum phase delay Δt_{phase} is below one femtosecond and the period of light is about 5 femtoseconds at 1500-nm wavelength. (ii) Generally, an additional phase delay can arise due to the interfaces between air/metamaterial and metamaterial/substrate. Thus, the experiments must be accompanied by transmittance/reflectance spectroscopy and by theory to ensure that these phase factors do not dominate over those due to propagation (see below). This interface aspect can generally also influence the group delay, but turns out to be unimportant here.

Figure 3 shows results obtained on a negative-index metamaterial. By laterally translating the sample (Fig. 1D), we first measure the air interferogram, then that of the sample. The glass substrate is in the optical path in either case, hence it drops out when considering the difference. The zero of the interferometer time-delay axis is set to be at the maximum of the air interferogram. We measure one air interferogram within about 2 s acquisition time, then we move the sample in by computer control, take a second interferogram, move the sample out again, and

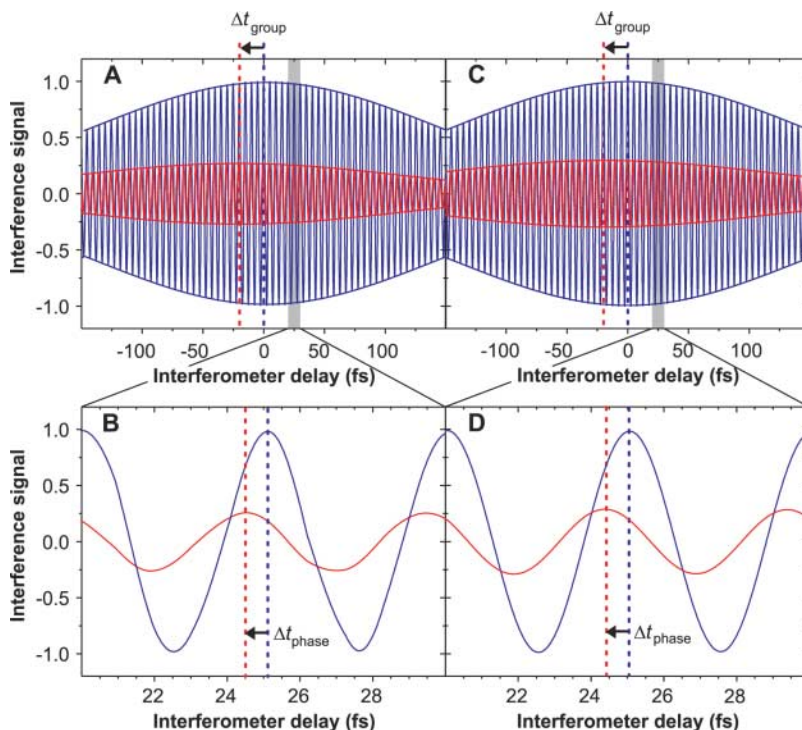


Fig. 3. (A) Examples of typical measured interferograms (constant background subtracted for clarity), air interferogram (blue), and interferogram with sample (red). The sample corresponds to Fig. 1, the OPO wavelength is 1500 nm. The Gaussian envelopes obtained from a least-squares fit to the interferogram extrema are depicted for both cases. The resulting negative group delay Δt_{group} is indicated. (B) Enlarged view of two individual interference fringes, the resulting negative phase delay Δt_{phase} is indicated. The corresponding calculated data are shown in (C) and (D).

repeat the entire procedure 20 times. In this fashion, we can identify possible drifts of our setup. Typically, we find drifts smaller than 100 attoseconds throughout the procedure. Each of the two interferograms shown in Fig. 3A results from averaging 20 individual scans with a total acquisition time of 40 s. When inserting a sample with thickness d and refractive index n , $v_{\text{phase}} = c_0/\text{Re}(n)$, and the phase time delay $\Delta t_{\text{phase}} = 2d/v_{\text{phase}} - 2d/c_0$ results, where $c_0 = 2.99 \times 10^8$ m/s is the vacuum velocity of light. The factor of 2 stems from the double-pass geometry in the Michelson interferometer (Fig. 1D). Similarly, we get the group time delay $\Delta t_{\text{group}} = 2d/v_{\text{group}} - 2d/c_0$. For the example depicted in Fig. 4, we have $\Delta t_{\text{phase}} = -0.62$ fs < 0 and $\Delta t_{\text{group}} = -19.1$ fs < 0 . The error in determining Δt_{phase} is 0.07 fs, the error in Δt_{group} is 0.3 fs. To test our apparatus, we also performed experiments on a $d = 120$ nm thin dielectric film of HfO_2 with real refractive index $n = +1.95$ on glass substrate, leading to positive

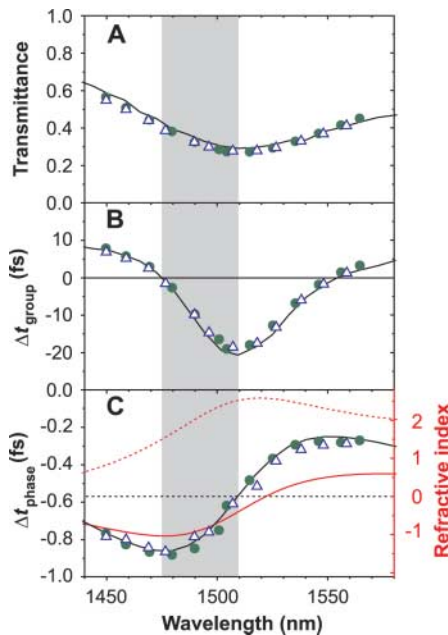


Fig. 4. Summary of two different sets of experiments (blue triangles and green circles) on the sample corresponding to Figs. 1 and 2. The black curves are calculated data. (A) Transmittance spectra measured with the OPO. (B) Group delay Δt_{group} (compare to Fig. 3). (C) Phase delay Δt_{phase} . A refractive index of $\text{Re}(n) = 0$ together with the sample thickness of $d = 85$ nm corresponds to a propagation phase delay of $-2 \times 85 \text{ nm}/c_0 = -0.57$ fs. This condition is given by the dashed horizontal line. (C) also reveals the real (solid) and imaginary (dashed) part of the refractive index (red scale at right), as retrieved from the data of Fig. 2. The gray area highlights the regime where simultaneously $v_{\text{phase}} < 0$ and $v_{\text{group}} < 0$.

phase delay $\Delta t_{\text{phase}} = +0.79$ fs > 0 and positive group delay $\Delta t_{\text{group}} = +0.78$ fs > 0 . Here, phase and group delay are identical within the measurement error and consistent with the HfO_2 refractive index.

Figure 4 summarizes measured phase and group delays for various OPO center wavelengths, individually obtained along the lines of Fig. 3. The phase delay Δt_{phase} is negative for the entire spectral range depicted. The group delay is either negative or positive. All measurements agree very well with our calculations, which use the identical sample parameters as in Fig. 2. These calculations directly simulate the experiment (Fig. 3, C and D). We let a 170-fs Gaussian pulse propagate through the structure shown in Fig. 1, but we do not use the retrieved effective material parameters. However, using the retrieved material parameters would give strictly the identical result, because the complex transmittance and reflectance coefficients are strictly identical, owing to the principle of the retrieval procedure (18).

We start our discussion of the data in Fig. 4C by assuming that the phase delay is exclusively due to propagation. In this case, a negative refractive index requires phase delays more negative than $\Delta t_{\text{phase}} = 0 - 2d/c_0$. With the metamaterial thickness of $d = 85$ nm, we get the $\text{Re}(n) = 0$ line at $\Delta t_{\text{phase}} = -0.57$ fs, which is illustrated by the dashed horizontal line in Fig. 4C. However, if the phase delay was exclusively due to propagation, the crossing of the phase-delay curve with the $\text{Re}(n) = 0$ line and the zero crossing of the real part of the retrieved refractive index in Fig. 4C should strictly coincide. We find a small spectral shift between the two crossings. This shift originates from an additional phase delay due to the interfaces between air/metamaterial and metamaterial/substrate. At these interfaces, one obtains phase factors from the Fresnel equations for complex metamaterial impedances. Multiple reflections between these interfaces further modify the phase.

It is simple to understand the measured sign of the group delay in terms of an effective material (Fig. 4B). The group velocity v_{group} can be expressed as

$$v_{\text{group}} = \frac{d\omega}{dk} = \frac{c_0}{\text{Re}(n) + \omega \frac{d \text{Re}(n)}{d\omega}}$$

For the fictitious case of negligible dispersion, the group velocity is identical to the phase velocity, i.e., the group velocity is negative if the phase velocity (equivalently the real part of the refractive index) is negative. In the presence of dispersion, the second term in the denominator can be either positive or negative, depending on which part of the spectral resonance is considered. For frequen-

cies where the derivative of the index with respect to frequency is positive (Fig. 4C, right side), the second term can overcompensate the negative refractive index. This can lead to a positive group velocity, hence to a positive group delay. Our direct experiments are consistent with indirect experiments on negative-index metamaterials in the microwave regime (19), where the group delay was calculated numerically on a computer from the measured dispersion of the phase delay.

We have shown in direct pulse propagation experiments on negative-index metamaterials that the phase velocity can be negative. Furthermore, contrary to common intuition, the group velocity can also be negative simultaneously. For other spectral positions, we find negative phase velocity and positive group velocity. For all sign combinations of phase and group velocity in effective metamaterials, the Poynting vector is positive—otherwise no signal would be transmitted through the sample.

References and Notes

1. L. Brillouin, *Wave Propagation and Group Velocity* (Academic, New York, 1960).
2. C. G. B. Garrett, D. E. McCumber, *Phys. Rev. A* **1**, 305 (1970).
3. S. Chu, S. Wong, *Phys. Rev. Lett.* **48**, 738 (1982).
4. L. J. Wang, A. Kuzmich, A. Dogarlu, *Nature* **406**, 277 (2000).
5. M. D. Stenner, D. J. Gauthier, M. A. Neifeld, *Nature* **425**, 695 (2003).
6. M. S. Bigelow, N. N. Lepeshkin, R. W. Boyd, *Science* **301**, 200 (2003).
7. R. A. Shelby, D. R. Smith, S. Schultz, *Science* **292**, 77 (2001).
8. D. R. Smith, J. B. Pendry, M. C. K. Wiltshire, *Science* **305**, 788 (2004).
9. S. Linden et al., *Science* **306**, 1351 (2004).
10. S. Zhang et al., *Opt. Express* **13**, 4922 (2005).
11. S. Zhang et al., *Phys. Rev. Lett.* **95**, 137404 (2005).
12. N. Grigorenko et al., *Nature* **438**, 335 (2005).
13. G. Dolling et al., *Opt. Lett.* **30**, 3198 (2005).
14. V. M. Shalaev et al., *Opt. Lett.* **30**, 3356 (2005).
15. V. G. Veselago, *Sov. Phys. Usp.* **10**, 509 (1968).
16. The calculations are based on a finite-difference time-domain approach and use the commercial software package CST Microwave Studio.
17. P. B. Johnson, R. W. Christy, *Phys. Rev. B* **6**, 4370 (1972).
18. Th. Koschny et al., *Phys. Rev. B* **71**, 245105 (2005).
19. J. F. Woodley, M. Mojahedi, *Phys. Rev. E* **70**, 046603 (2004).
20. We thank Th. Koschny for stimulating discussions. We acknowledge support by the Deutsche Forschungsgemeinschaft (DFG) and the State of Baden-Württemberg through the DFG-Center for Functional Nanostructures within subproject A1.5. The research of M.W. is further supported by project DFG-We 1497/9-1 and that of S.L. through a Helmholtz-Hochschul-Nachwuchsgruppe (VH-NG-232). The research of C.M.S. is further supported by the Alexander von Humboldt senior-scientist award 2002, by Ames Laboratory (Contract No. W-7405-Eng-82), European Union projects DALHM, PHOREMOST, METAMORPHOSE, and by the Defense Advanced Research Projects Agency (HR0011-05-C-0068).